Optimal Closed-Loop Control of the Azimuthal Velocity Profile by E×B Actuation in HELCAT

Zeki Okan Ilhan[1], David Huxley-Cohen[1], Hexiang Wang[1], Eugenio Schuster[1], Mark Gilmore[2], Andrew Ware[3]
[1]Lehigh University, Bethlehem, PA, USA
[2]University of New Mexico, Albuquerque, NM, USA
[3]University of Montana, Missoula, MT, USA
e-mail: zoi210@lehigh.edu

***Abstract*— The cross-field turbulence-driven particle transport in magnetically confined plasmas can be reduced by adequately shaping the flow profiles. HELCAT (HELicon-CAThode), a linear magnetized plasma device, uses concentric ring electrodes to modify the flow profiles by E×B actuation. As a result, turbulent particle and heat transport can be mitigated by generating a sheared radial electric field through the varying ring voltages. Active control of the turbulent fluctuations, including the associated cross-field particle transport, via manipulation of flow profiles is investigated in this work. Once a desired radial azimuthal velocity profile, and its associated level of turbulent fluctuations, are identified, the challenge of systematically achieving and sustaining it still remains. A model-based feedback controller is proposed to achieve this goal even in the presence of external disturbances, model uncertainties and perturbed initial conditions. A linear-quadratic-integral (LQI) optimal controller is designed to minimize a weighted combination of the tracking error and the control effort. Numerical simulations show the effectiveness of the proposed controller to regulate the radial azimuthal velocity profile around a prescribed desired profile. The proposed control solution has the potential of being used as a systematic tool to elucidate the physics of laboratory plasmas such as those achieved in HELCAT.**

I. Introduction

Nowadays, laboratory plasma physics has found applications in various research areas ranging from solar corona heating and laboratory astrophysics to plasma nonlinear dynamics and turbulence control mechanisms. Plasma experiments in this wide range of application areas need a plasma source that can generate a broad plasma parameter space with a plasma duration of several miliseconds [1]. For this purpose, the HELCAT dual-source linear plasma device, which utilizes both helicon and thermionic cathode sources, has been created. The helicon plasmas are characterized by their high density, relatively longer discharge times, and peaked profiles, whereas the cathode plasmas typically have lower density, short discharge time, and broader profiles. Combining the two plasma sources of different character, HELCAT is capable of addressing various plasma phenomena in the same machine [1].

In this work, the attention is focused on the control of the turbulence-driven particle transport in HELCAT. The control elements in HELCAT are a set of biased concentric ring electrodes that terminate the plasma column. It has been shown that by varying the bias of these ring electrodes, it is possible to manipulate the resulting $E \times B$ flow profile (i.e., the poloidal or azimuthal flow, V_θ) [2]. The radial derivative of the azimuthal flow (i.e., the flow shear), has been shown effective in increasing or decreasing the drift wave turbulence at the plasma edge. Hence, the turbulent fluctuations may be controlled indirectly in HELCAT by controlling the azimuthal flow profile evolution, $V_\theta(r,t)$.

Both open-loop and closed-loop approaches are possible for controlling the azimuthal flow in HELCAT. So far, the authors have focused on an open loop control approach based on the extremum seeking algorithm, which is shown effective for both fluctuation mitigation [3] and azimuthal flow regulation [4]. The main advantage of the open-loop approach is the possibility of utilizing highly complex transport models since the controller is computed off-line. On the other hand, the main drawback of the open-loop approach is that it is highly sensitive to disturbances and modeling uncertainties.

In this paper, a closed-loop approach based on the linear-quadratic-integral (LQI) optimal control theory is proposed. The proposed closed-loop controller is capable of coping with various model uncertainties as well as rejecting a nonlinear disturbance affecting the azimuthal flow profile, $V_\theta(r,t)$, dynamics. Since the closed-loop control must be computed on-line, a reduced-order, control-oriented model is also proposed to replace the highly complex "TransportHelicon" code under development for HELCAT. The effectiveness of the proposed feedback controller is shown using numerical simulations.

The organization of this paper is as follows. The partial differential equation (PDE) model governing the azimuthal flow profile evolution in HELCAT is briefly introduced in Section II. This main model is reduced to a finite-dimensional, control-oriented model in Section III using the truncated Taylor series expansion method. The design of a LQI optimal feedback controller for the regulation of the azimuthal flow profile around a desired target profile is described in Section IV. In Section V, the proposed controller is then tested in simulations based on the complete PDE model. Finally, conclusions and future work are stated in Section VI.

This work was supported by the National Science Foundation (PHY-0903803) and the US Department of Energy (DE-FG02-09ER55022).

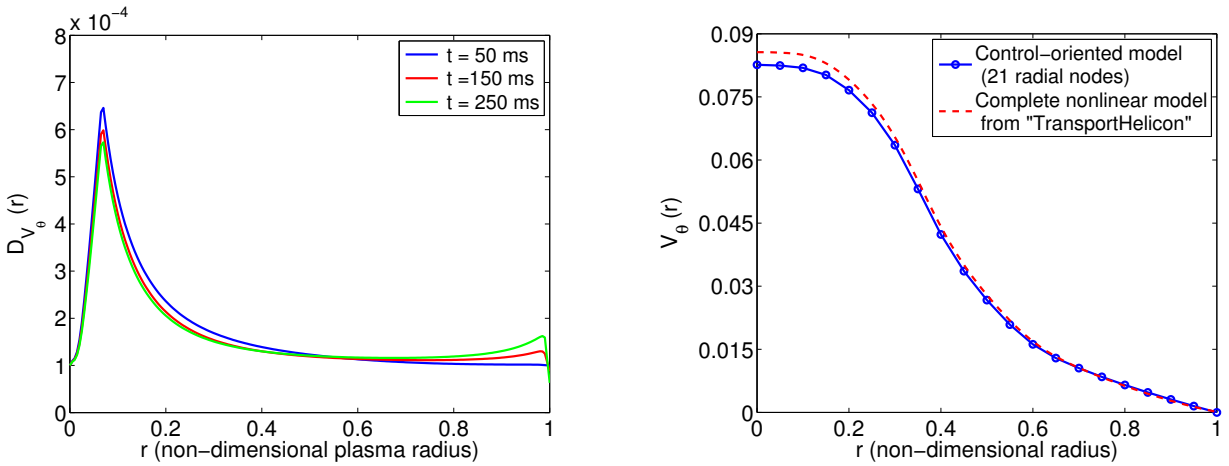

(a) (b)

Fig. 1. (a) Azimuthal flow diffusivity profiles extracted at different instants. (b) V_θ flow profiles at $t = 250$ ms for $p_c = [25, 10, 20, -10, 0, -5]$.

II. Azimuthal Flow Evolution Model

Based on [5], the radial-temporal evolution of the axially averaged azimuthal flow $V_\theta(r,t)$ is governed by a PDE model ($t \geq 0$, $r \in [0,1]$) given by

$$\frac{\partial V_\theta}{\partial t} = S_\theta - \mu V_\theta + \frac{1}{r}\frac{\partial}{\partial r}\left[rD_{V_\theta}\frac{\partial V_\theta}{\partial r}\right] + \underbrace{\alpha_\theta \frac{\partial}{\partial r}\left[r^2\epsilon\frac{\partial \epsilon}{\partial r}\frac{\partial E_r}{\partial r}\right]\left(\frac{2}{r^2 f_{ac}}\right)}_{\textbf{Reynolds stress flow drive (nonlinear)}}, \quad (1)$$

where $S_\theta(r)$ is an external azimuthal flow (momentum) source, $D_{V_\theta}(r,t)$ is the azimuthal flow diffusivity, $\epsilon(r,t)$ is the plasma RMS fluctuation level, $E_r(r,t)$ is the radial electric field profile and $f_{ac}(r)$ is the Reynolds Stress suppression term. The model constants appearing on the right hand side of (1) are the flow damping multiplier, μ, and the coefficient of Reynolds Stress flow generation, α_θ.

The control elements are the biased concentric rings in the actual HELCAT device [4]. Their effect is modeled as localized Gaussian momentum sources in the predictive transport code ("TransportHelicon") under development for HELCAT based on the work in [5]. The effect will be identical to a source of poloidal $E \times B$ flow when diamagnetic flows are negligible [3]. Hence, the external azimuthal momentum source from the rings is modeled as

$$S_\theta(r) = \sum_{j=1}^{6} p_c(j)\, e^{\frac{-(r_p(j)-r)^2}{2w_{pc}(j)^2}}, \quad (2)$$

where the input array $p_c \in \mathbb{R}^{6\times 1}$ denotes the momentum source strengths, and the constant arrays $r_p \in \mathbb{R}^{6\times 1}$ and $w_{pc} \in \mathbb{R}^{6\times 1}$ represent the radial locations and the radial widths of the Gaussian momentum sources, respectively.

On the RHS of (1), the diffusivity of the azimuthal velocity, $D_{V_\theta}(r,t)$, is modeled as

$$D_{V_\theta}(r,t) = 10D_0 + 50D_{0b}\sqrt{\frac{T_e}{\left|\frac{1}{T_e}\frac{\partial T_e}{\partial r} + \frac{1}{n}\frac{\partial n}{\partial r}\right|}}\,\epsilon^2\,\mu_{\text{prof}}, \quad (3)$$

where the collisional particle transport coefficient D_0, the turbulent particle transport coefficient D_{0b}, and the turbulent transport profile modification μ_{prof} are all constants, and where $T_e(r,t)$ and $n(r,t)$ represent the plasma electron temperature and density profiles, respectively. Also, the Reynolds stress suppression term, f_{ac}, is defined as

$$f_{ac}(r) = 1 + 10^{-6}\left[\frac{1}{(1.000001 - r)^6} + \frac{1}{(0.000001 + r)^6}\right]. \quad (4)$$

Note that the highly nonlinear last term appearing on the RHS of (1) physically models the Reynolds stress flow drive. Hence, in the absence of the external momentum source effect (S_θ), the generation of flow is mainly a competition between the Reynolds stress flow drive (fourth term on the RHS of (1)) and both magnetic damping (second term on the RHS of (1)) and momentum diffusion (third term on the RHS of (1)).

III. Control-Oriented Model via Truncated Taylor Series

The nonlinear term associated with the Reynolds stress flow drive is bounded, i.e.,

$$|W(r,t)| = \left|\alpha_\theta \frac{\partial}{\partial r}\left[r^2\epsilon\frac{\partial \epsilon}{\partial r}\frac{\partial E_r}{\partial r}\right]\left(\frac{2}{r^2 f_{ac}}\right)\right| \leq M. \quad (5)$$

Hence, from the control point of view, it is considered as a *bounded nonlinear disturbance* in this work. The disturbance-free azimuthal flow response model can then be represented by the following PDE

$$\frac{\partial V_\theta}{\partial t} = S_\theta(r) - \mu V_\theta + \frac{1}{r}\frac{\partial}{\partial r}\left(rD_{V_\theta}(r,t)\frac{\partial V_\theta}{\partial r}\right), \quad (6)$$

with the imposed boundary conditions

$$\frac{\partial V_\theta}{\partial r}(0,t) = 0 \;\;,\;\; V_\theta(1,t) = 0, \quad (7)$$

and a predefined initial condition

$$V_\theta(r,0) = V_{\theta_0}(r). \quad (8)$$

The azimuthal flow diffusivity D_{V_θ} in (6) is both time and space dependent. Fig. 1(a) shows the radial profile of D_{V_θ} at different instants throughout the 250 ms discharge as extracted from the predictive "TransportHelicon" code for HELCAT. The profiles in Fig. 1(a) are similar in shape and do not vary much as time evolves. Hence, the profile at $t = 150$ ms can be used to approximate D_{V_θ} as a time-independent, radially-varying term, i.e.,

$$D_{V_\theta}(r,t) \approx \hat{D}_{V_\theta}(r) = D_{V_\theta}(r,t)|_{t=150\text{ms}}\,. \tag{9}$$

Using the approximation (9), the RHS of (6) can be expanded according to the chain rule as follows

$$\frac{\partial V_\theta}{\partial t} = S_\theta - \mu V_\theta + \left(\frac{1}{r}\hat{D}_{V_\theta} + \frac{\partial \hat{D}_{V_\theta}}{\partial r}\right)\frac{\partial V_\theta}{\partial r} + \hat{D}_{V_\theta}\frac{\partial^2 V_\theta}{\partial r^2}. \tag{10}$$

To construct a reduced-order model suitable for control design, the governing PDE (10) is discretized in space using a truncated Taylor series expansion, which approximates the spatial derivatives while leaving the time domain continuous [6]. The non-dimensional domain of interest, $r \in [0,1]$, can be divided into l nodes. Hence, the spacing between the nodes, h, becomes $h = 1/(l-1)$. The interior node region, $2 \le i \le (l-1)$, uses central finite difference spatial derivative approximations of $O(h^2)$. The left boundary node, $i = 1$, uses forward finite difference spatial derivative approximation of $O(h^2)$, while the right boundary node, $i = l$, is fixed by the Drichlet boundary condition imposed at $r = 1$

The infinite-dimensional azimuthal flow model (10) can then be discretized in space using the aforementioned finite difference approximations together with the imposed boundary conditions (7). The resulting reduced-order, control-oriented model can be represented compactly in the standard linear, time-invariant, state-space form

$$\dot{x}(t) = Ax(t) + Bu(t), \tag{11}$$

where $x(t) = [V_{\theta_2}(t), V_{\theta_3}(t), ..., V_{\theta_{l-1}}(t)]^T \in \mathbb{R}^{n\times 1}$ is the state vector containing the values of $V_\theta(r,t)$ at the $n = l-2$ interior nodes, the input vector $u(t) = [p_c(1), p_c(2), .., p_c(6)]^T \in \mathbb{R}^{6\times 1}$ is the array of azimuthal momentum source strengths, $A \in \mathbb{R}^{n\times n}$ and $B \in \mathbb{R}^{n\times 6}$ are constant system matrices.

The elements of the state matrix A for the interior node $i = 2$ are given by

$$A_{1,1} = \frac{4}{3}\left[\frac{\hat{D}_2}{h^2} - \frac{1}{2h}\left(\frac{\hat{D}_2}{h} + \frac{\hat{D}_3 - \hat{D}_1}{2h}\right)\right] - \mu - 2\frac{\hat{D}_2}{h^2}, \tag{12}$$

$$A_{1,2} = \frac{2}{3}\frac{\hat{D}_2}{h^2} + \frac{4}{3}\frac{1}{2h}\left(\frac{\hat{D}_2}{h} + \frac{\hat{D}_3 - \hat{D}_1}{2h}\right), \tag{13}$$

where $\hat{D}_i = \hat{D}_{V_\theta}(r_i)$ represents the discrete version of the radially-varying, approximate diffusivity term, (9). Similarly, the elements of the A matrix for the interior region, $3 \le i \le (l-2)$, are given by

$$A_{i-1,i-2} = \frac{\hat{D}_i}{h^2} - \frac{1}{2h}\left(\frac{\hat{D}_i}{(i-1)h} + \frac{\hat{D}_{i+1} - \hat{D}_{i-1}}{2h}\right), \tag{14}$$

$$A_{i-1,i-1} = -\mu - 2\frac{\hat{D}_i}{h^2}, \tag{15}$$

$$A_{i-1,i} = \frac{\hat{D}_i}{h^2} + \frac{1}{2h}\left(\frac{\hat{D}_i}{(i-1)h} + \frac{\hat{D}_{i+1} - \hat{D}_{i-1}}{2h}\right). \tag{16}$$

The elements for the interior node $i = l-1$ are given by

$$A_{n,n-1} = \frac{\hat{D}_{l-2}}{h^2} - \frac{1}{2h}\left(\frac{\hat{D}_{l-2}}{(l-3)h} + \frac{\hat{D}_{l-1} - \hat{D}_{l-3}}{2h}\right), \tag{17}$$

$$A_{n,n} = -\mu - 2\frac{\hat{D}_{l-2}}{h^2}. \tag{18}$$

The remaining entries of the state matrix A are all zero. Since the values of V_θ at the boundary nodes $i = 1$ and $i = l$ are known from the boundary conditions, they are not considered as the states for the control-oriented model (11).

The input matrix B in (11) models the azimuthal flow source term, S_θ in (6). Hence, for l radial nodes, (i.e., $n = l-2$ states), the elements of $B \in \mathbb{R}^{n\times 6}$ are obtained directly from the discrete version of the source model (2) as

$$B_{j,k} = \exp\left\{-\frac{[r_p(k) - (j-1)h]^2}{2\,[w_{pc}(k)]^2}\right\}, \tag{19}$$

where $j = 1, 2, ..., n$ and $k = 1, 2, ..., 6$. The reduced-order, linear state-space model (11) is generated for $l = 21$ nodes, (i.e., $n = 19$ states) and then compared with the actual nonlinear PDE (1), which is simulated using the predictive "TransportHelicon" code for HELCAT. The radial V_θ flow profiles obtained from the two models are then compared in Fig. 1(b). Although the state-space model (11) does not take into account the nonlinear Reynolds stress flow drive term, it captures the main dynamics of the overall nonlinear V_θ flow model and hence is useful for feedback control design.

Note that the complete V_θ flow model (1) combines the disturbance-free model (6) with the Reynolds stress flow drive, which is considered in this paper as a bounded, nonlinear disturbance acting on the reduced-order model (11). Hence, the finite-dimensional form of the complete V_θ flow model (1) can be put into the following state-space model

$$\dot{x}(t) = Ax(t) + Bu(t) + w(t), \tag{20}$$

where the vector $w(t) = [W_2(t), W_3(t), ..., W_{l-1}(t)]^T \in \mathbb{R}^{n\times 1}$ lists the value of the unknown but bounded disturbance, $W(r,t)$ at the $n = l-2$ interior nodes.

IV. Controller Synthesis

A. Optimal Tracking Control Problem Statement

In addition to the state equation (20), an output equation can be defined to provide a linear combination of the states. The overall plant is then characterized by the following multi input, multi output (MIMO) system

$$\dot{x}(t) = Ax(t) + Bu(t) + w(t), \tag{21}$$

$$y(t) = Cx(t), \tag{22}$$

where $C \in \mathbb{R}^{m\times n}$ is the output matrix and $y(t) \in \mathbb{R}^{m\times 1}$ is the output vector. The control objective is to make the

output $y(t)$ track a constant reference z *as closely as possible* during the time interval $[0, t_f]$ with *minimum control effort.* Hence, for this application, the tracking error, $e(t) \in \mathbb{R}^{m\times 1}$, is defined as

$$e(t) = y(t) - z = Cx(t) - z. \tag{23}$$

To minimize a weighted combination of the tracking error and control energy, one can consider the standard, quadratic performance index

$$\min_{u(t)} J = \frac{1}{2} e^T(t_f) P(t_f) e(t_f) + \frac{1}{2}\int_0^{t_f} \left[e^T(t) Q e(t) + u^{*T}(t) R u^*(t) \right] dt, \tag{24}$$

where $Q \in \mathbb{R}^{m\times m}$ and $R \in \mathbb{R}^{m\times m}$ are symmetric, positive definite matrices and $P(t_f) \in \mathbb{R}^{m\times m}$. The disturbance-free plant

$$\dot{x}(t) = Ax(t) + Bu(t) \tag{25}$$

$$y(t) = Cx(t), \tag{26}$$

together with equations (23)-(24) define a standard Linear-Quadratic-Tracking (LQT) optimal control problem, the solution of which is in state-feedback form utilizing the time-varying Kalman Gain [7]. However, the resulting system will produce some offset error while tracking the constant reference. To improve the tracking performance of the closed-loop system and reject the effect of the disturbance, integral action should be added to the optimal control law.

B. Linear-Quadratic-Integral (LQI) Optimal Controller

The LQI Optimal Controller is considered here since it adds the integral action to the standard LQT problem described in the previous section. The LQI controller is designed based on the disturbance-free model (25)-(26). The resulting closed-loop system is insensitive to slowly-varying, unknown process disturbance ($w(t)$ in (21)) while tracking a constant reference. To obtain the LQI controller, the quadratic performance index (24) is modified as

$$\min_{v(t)} J = \frac{1}{2} e^T(t_f) P(t_f) e(t_f) + \frac{1}{2}\int_0^{t_f} \left[e^T(t) Q e(t) + v^{*T}(t) R v^*(t) \right] dt, \tag{27}$$

where $v(t)$ is the time derivative of the actual control input $u(t)$, i.e.,

$$v(t) = \frac{du(t)}{dt}. \tag{28}$$

Also, the augmented state vector $\tilde{x}(t) \in \mathbb{R}^{m+n}$ is introduced

$$\widetilde{x}(t) = \begin{bmatrix} e(t) \\ \hline \dot{x}(t) \end{bmatrix}. \tag{29}$$

Differentiating (23),

$$\dot{e}(t) = C\dot{x}(t). \tag{30}$$

Similarly, from (25) and (28),

$$\ddot{x}(t) = A\dot{x}(t) + B\frac{du(t)}{dt} = A\dot{x}(t) + Bv(t). \tag{31}$$

Substituting (30) and (31) into (29), the time derivative of the augmented state vector, $\tilde{x}(t)$, becomes

$$\frac{d\widetilde{x}(t)}{dt} = \frac{d}{dt}\begin{bmatrix} e(t) \\ \dot{x}(t) \end{bmatrix} = \begin{bmatrix} 0 & C \\ 0 & A \end{bmatrix}\begin{bmatrix} e(t) \\ \dot{x}(t) \end{bmatrix} + \begin{bmatrix} 0 \\ B \end{bmatrix} v(t). \tag{32}$$

Based on (32), augmented matrices can be defined as

$$\widetilde{A} = \begin{bmatrix} 0_{m\times m} & C_{m\times n} \\ 0_{n\times m} & A_{n\times n} \end{bmatrix}, \ \widetilde{B} = \begin{bmatrix} 0_{m\times m} \\ B_{n\times m} \end{bmatrix}. \tag{33}$$

Hence, the state equation for the enlarged $m+n$ dimensional system (32) can be rewritten as

$$\frac{d\widetilde{x}(t)}{dt} = \widetilde{A}\widetilde{x}(t) + \widetilde{B}v(t). \tag{34}$$

Note also that the performance index (27) can be expressed in terms of the enlarged system (34) as

$$\min_{v(t)} J = \frac{1}{2}\widetilde{x}^T(t_f)\widetilde{P}(t_f)\widetilde{x}(t_f) + \frac{1}{2}\int_0^{t_f} \left[\widetilde{x}^T(t)\widetilde{Q}\widetilde{x}(t) + v^{*T}(t) R v^*(t) \right] dt, \tag{35}$$

where the augmented weight matrices are

$$\widetilde{P}(t_f) = \begin{bmatrix} P_{m\times m} & 0_{m\times n} \\ 0_{n\times m} & 0_{n\times n} \end{bmatrix}, \ \widetilde{Q} = \begin{bmatrix} Q_{m\times m} & 0_{m\times n} \\ 0_{n\times m} & 0_{n\times n} \end{bmatrix}. \tag{36}$$

Note that (34) and (35) define a standard Linear-Quadratic-Regulator (LQR) problem, the solution of which yields a time-variant state-feedback of the form

$$v^*(t) = -K(t)\widetilde{x}(t), \tag{37}$$

where $K(t) \in \mathbb{R}^{m\times(m+n)}$ is the *Kalman Gain* given by

$$K(t) = R^{-1}\widetilde{B}^T\widetilde{P}(t), \tag{38}$$

and $\widetilde{P}(t)$ is the solution of the matrix Ricatti Differential Equation (RDE)

$$-\dot{\widetilde{P}}(t) = \widetilde{A}^T\widetilde{P}(t) + \widetilde{P}(t)\widetilde{A} - \widetilde{P}(t)\widetilde{B}R^{-1}\widetilde{B}^T\widetilde{P}(t) + \widetilde{Q} \tag{39}$$

subject to the final condition $\widetilde{P}(t_f)$ [7]. If the controllability and observability conditions are satisfied for $(\widetilde{A}, \widetilde{B})$ and $(\widetilde{A}, \widetilde{Q}^{\frac{1}{2}})$, respectively, then for every choice of $\widetilde{P}(t_f)$, there exists a constant, stationary matrix $\widetilde{P}_+$ that satisfies the RDE (39) in the limit as $t \to 0$. Furthermore, $\widetilde{P}_+$ is the unique positive definite solution to the Algebraic Ricatti Equation (ARE)

$$0 = \widetilde{A}^T\widetilde{P}_\infty + \widetilde{P}_\infty\widetilde{A} - \widetilde{P}_\infty\widetilde{B}R^{-1}\widetilde{B}^T\widetilde{P}_\infty + \widetilde{Q}. \tag{40}$$

In this case, the time-variant Kalman Gain (38) can be approximated by the constant gain K, which is given by

$$\begin{aligned} K &= R^{-1}\widetilde{B}^T\widetilde{P}_+ \\ &= [K_I \ \ K_P] \\ &= \begin{bmatrix} R^{-1}B^T\widetilde{P}_{21} & R^{-1}B^T\widetilde{P}_{22} \end{bmatrix}, \end{aligned} \tag{41}$$

where $\widetilde{P}_{21} \in \mathbb{R}^{n\times m}$ and $\widetilde{P}_{22} \in \mathbb{R}^{n\times n}$ are partitions of $\widetilde{P}_+ \in \mathbb{R}^{(m+n)\times(m+n)}$ given by

$$\widetilde{P}_+ = \begin{bmatrix} \widetilde{P}_{11} & \widetilde{P}_{12} \\ \widetilde{P}_{21} & \widetilde{P}_{22} \end{bmatrix}. \tag{42}$$

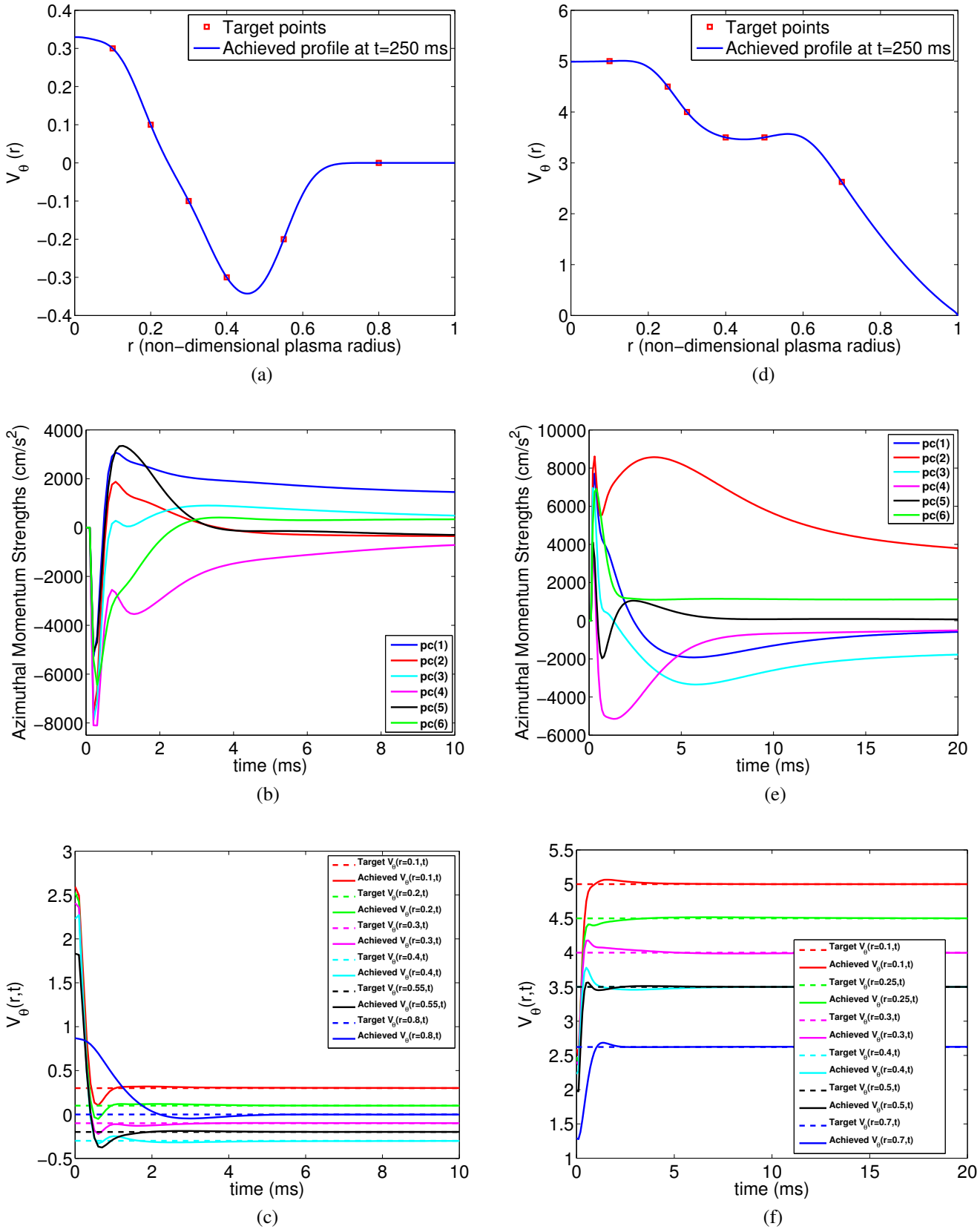

Fig. 2. Results of the two different reference tracking simulation studies: (a)-(c) and (d)-(f), respectively. (a) & (d): Comparisons of the target and achieved $V_\theta(r)$ flow profiles at $t_f = 250$ ms (b) & (e): Time evolution of the optimal inputs, (c) & (f): Time evolution of the outputs.

Note from (41) that the first element of the K matrix, i.e., $K_I \in \mathbb{R}^{m\times m}$ represents the integral gain and the second element, $K_P \in \mathbb{R}^{m\times n}$ gives the proportional state feedback gain. Using the constant gain K in (37), the optimal feedback control law $v^*(t)$ for the enlarged system (34) becomes

$$\begin{aligned} v^*(t) = -K\widetilde{x}(t) &= -[K_I \;\; K_P] \begin{bmatrix} e(t) \\ \dot{x}(t) \end{bmatrix} \\ &= -K_I e(t) - K_P \dot{x}(t) \end{aligned} \tag{43}$$

Integrating (43) from the initial time $t = 0$ to any time t, the optimal feedback control law, $u^*(t)$, for the actual system (21)-(22) can be expressed as

$$u^*(t) = -K_I \int_0^t e(\tau) d\tau - K_P \left[x(t) - x_0\right], \tag{44}$$

where $x_0 = x(t = 0)$ is the initial condition for the state vector and the constant control gains are

$$K_I = R^{-1} B^T \widetilde{P}_{21} \qquad K_P = R^{-1} B^T \widetilde{P}_{22}. \tag{45}$$

Finally, substituting the tracking error, $e(t)$, (i.e., equation (23)) back into (44), the optimal LQI feedback control law can be expressed in terms of the state and reference as

$$u^*(t) = -K_I \int_0^t \left[Cx(\tau) - z\right] d\tau - K_P \left[x(t) - x_0\right]. \tag{46}$$

Note that the optimal solution (46) yields a PI (proportional plus integral) control law.

V. Simulation Study

For $l = 21$ radial nodes, (i.e., $n = 19$ states), the controllability and observability conditions discussed in the previous section are satisfied when setting $m = 6$. In this way, the MIMO model (21)-(22) becomes perfectly square, having same number of inputs and outputs.

The constant weight matrices of the LQI performance index (27) are defined as $Q = 100\, I_{6\times 6}$, and $R = 0.001\, I_{6\times 6}$, where I is the identity matrix. The final value of the time dependent matrix, $P(t_f) \in \mathbb{R}^{6\times 6}$, is taken as zero in this design. The ARE equation (40) is solved in MATLAB to obtain the proportional and integral control gains, K_p and K_I. The proposed LQI controller (46) is then implemented in the predictive transport code, "TransportHelicon", to simulate the complete nonlinear PDE (1) governing the evolution of the V_θ flow up to 250 ms

Due to controllability constraints, only 6 out of the 19 states can be forced to track a constant reference. Hence, one can achieve V_θ flow control only at 6 points along the plasma radius. The left and right columns of Fig. 2 summarize the results of two simulation studies where different reference profiles are tracked. The red squares in Fig. 2(a) and Fig. 2(d) show the 6 radial locations where profile control is achieved. Given a desired profile shape, one can pick those 6 locations carefully so that the resulting profile approaches the target profile as closely as possible. One can force different states (radial locations) to track the reference by adequately specifying the nonzero entries in the output matrix, C, in (22). As can be seen from Fig. 2(b) and Fig. 2(e), the 6 optimal inputs (i.e., the azimuthal momentum source strengths) are settling down within the first few miliseconds of the discharge, regulating the outputs around their desired values, as shown in Fig. 2(c) and Fig. 2(f), respectively.

VI. Conclusions and Future Work

The PDE governing the dynamics of the azimuthal flow has been first discretized using a truncated Taylor series expansion to generate a control-oriented, linear model in cascade with an unknown but bounded disturbance. An LQI optimal controller has been then designed based on the disturbance-free model. Numerical simulations show that the proposed controller is capable of tracking reference profiles while rejecting the small bounded disturbance, which reflects the effect of the Reynolds stress flow drive.

No restriction has been imposed so far on the actuators (momentum source strengths) in the predictive transport code. One of the future goals is to develop a physical model converting the bias ring voltages in the HELCAT device to the azimuthal momentum source strengths in the transport code. In this way, one could consider the saturation of the actuators during the control simulations since the voltage limits are well defined.

A multi-point probe capable of simultaneously measuring the azimuthal flow at various points along the plasma is currently under development. This probe will be useful in determining target azimuthal flow profiles corresponding to low levels of RMS fluctuations and will also enable the implementation of the designed LQI controller in the actual HELCAT device.

References

[1] A. G. Lynn, M. Gilmore, C. Watts, J. Herrea, R. Kelly, S. Will, S. Xie, L. Yan, and Y. Zhang, "The HelCat dual-source plasma device," *Review of Scientific Instruments*, vol. 80, no. 103501, 2009.

[2] N. Crocker, G. Y. Burin, M. J. Burin, G. R. Tynan, B. P. Cluggish, and K. R. Umstadter, "Control of Velocity Shear and Turbulence Through Biasing in CSDX," *Program of the 44th Annual Meeting of the APS Division of Plasma Physics*, vol. 47, p. 264, 2002.

[3] Q. Wang, E. Schuster, M. Gilmore, S. Xie, and A. Ware, "Extremum-Seeking-Based Fluctuation Mitigation by ExB Actuation in HELCAT," in *Proceedings of the 5th IEEE Multi-conference on Systems and Control, Denver, Colorado*, September 28-30 2011.

[4] Z. O. Ilhan, J. Barry, H. Wang, E. Schuster, M. Gilmore, and A. Ware, "Fluctuation Mitigation and Azimuthal Velocity Profile Regulation by Extremum Seeking in HELCAT," in *Proceedings of the 25th Symposium on Fusion Engineering, San Francisco, California*, June 11-14 2013.

[5] D. E. Newman, B. A. Carreras, D. Lopez-Bruna, P. H. Diamond, and V. B. Lebedev, "Dynamics and control of internal transport barriers in reversed shear discharges," *Physics of Plasmas*, vol. 5, no. 4, pp. 938–952, 1998.

[6] W. Schiesser, *The Numerical Method of Lines: Integration of Partial Differential Equations*. Academic Press, San Diego, 1991.

[7] D. Naidu, *Optimal Control Systems*. CRC Press, 2003.